RSC Sustainability

ROYAL SOCIETY OF CHEMISTRY

PAPER

View Article Online
View Journal | View Issue

Cite this: *RSC Sustainability*, 2023, **1**, 1511

Effective photocatalytic degradation of rhodamine-B over Zn-doped BaO_2 and SrO_2 composites under UV and sunlight irradiation†

Kirankumar Venkatesan Savunthari, [abc] Daneshwaran Balaji,[a] Nivedita Sudheer,[a] Mittal Bathwar,[a] Manjunath Rangasamy,[b] Ganesh Kumar Dhandabani, [d] Alain R. Puente Santiago, [e] Sumathi Shanmugam, *[a] Kien-Voon Kong *[b] and Vijayaraghavan R *[a]

Environmental pollution due to dye industries is a major concern as it affects both aquatic and human life. Among various processes, photocatalysis involving the advanced oxidation process (AOP) that employs semi-conductor based photocatalysis is popular and this process degrades dyes into CO_2 and H_2O. The currently used TiO_2 based photocatalysis requires ultra-violet (UV) light irradiation for activation. There is always a need for a catalyst that works under natural sunlight so that the dye degradation process is economical. Towards this objective, we have developed Zn doped metal peroxides as efficient photocatalysts towards rhodamine B (RhB) dye degradation. A new family of zinc-doped barium peroxide ($Ba_{1-x}Zn_xO_2$ $x = 0$, 0.2, 0.4, 0.6, and 0.8) and zinc-doped strontium peroxide ($Sr_{1-x}Zn_xO_2$ $x = 0$, 0.2, 0.4, 0.6, and 0.8) photocatalysts were prepared by the co-precipitation technique for the photocatalytic degradation of RhB under UV and natural sunlight irradiation. In particular, $Ba_{0.4}Zn_{0.6}O_2$ ($x = 0.6$) and $Sr_{0.6}Zn_{0.4}O_2$ ($x = 0.4$) photocatalysts exhibit higher photodegradation efficiency than the pure peroxides both under UV and sunlight irradiation. $Ba_{0.4}Zn_{0.6}O_2$ and $Sr_{0.6}Zn_{0.4}O_2$ photocatalysts show a degradation efficiency of 99.9% and 99.8% within 15 min and 10 min under UV light, respectively. The rate constants of degradation by doped peroxides, in particular $Ba_{0.4}Zn_{0.6}O_2$ and $Sr_{0.6}Zn_{0.4}O_2$, are 100 times higher than those of the parent peroxides.

Received 16th March 2023
Accepted 14th July 2023

DOI: 10.1039/d3su00091e

rsc.li/rscsus

Sustainability spotlight

Due to the rapid development of industry, environmental pollution has become a major topic worldwide. Water pollution is a key concern in the world today, posing a health risk to all living creatures. In particular, rhodamine B is commonly used as an organic dye and is extremely difficult to degrade under UV and natural sunlight. Consequently, developing novel catalysts to degrade rhodamine B under sunlight is an important topic. Here, we attempt to study effective photocatalysts (zinc-doped barium and strontium peroxide) for the degradation of rhodamine B under UV and sunlight. The synthesized photocatalysts exhibit a low bandgap and a high surface area, which helps degrade the rhodamine B dye in a short period under UV and sunlight irradiation. Furthermore, our research demonstrates an effective photocatalyst for persistent organic pollutants (POPs) that can be used for environmental remediation applications of sustainable development goals (SDGs).

Introduction

In recent decades, industrial activities have released uncontrolled amounts of persistent organic pollutants (POPs) caused by urbanization and population growth. Among industrial wastewater discharges, dye wastewater from the food, painting, paper, printing, and mining industries pollutes the environment.[1,2] These organic pollutants and dyes are vital pollutants which are highly toxic to aquatic life, and they affect plants and cause serious effects such as cancer.[3] The most common constituents of pollutants in wastewater are nitrophenol, methylene blue, rhodamine B and azo derivatives.[4–7] Rhodamine B (RhB), in particular, is one of the most commonly used

[a]*Department of Chemistry, School of Advanced Sciences, Vellore Institute of Technology, Vellore, Tamil Nadu 632014, India*

[b]*Department of Chemistry, National Taiwan University, Taipei 106, Taiwan*

[c]*Department of Chemistry and Chemical Biology, Northeastern University, Boston, Massachusetts 02115, USA*

[d]*Department of Pharmacy, National Taiwan University, Taipei 100, Taiwan*

[e]*Walker Department of Mechanical Engineering, University of Texas at Austin, Austin, TX 78712, USA*

† Electronic supplementary information (ESI) available. See DOI: https://doi.org/10.1039/d3su00091e

organic dyes. The International Agency for Research on Cancer (IARC) has classified rhodamine B (RhB), one of the most commonly used organic dyes, as a carcinogen.[8–11] RhB is commonly used in textiles, paper, printing and food items as a pigment. Its release into the environment as waste water causes serious health hazards due to its toxicity profile. It results in carcinogenicity and neurotoxicity. Some specific problems are nausea, vomiting, respiratory problems and gastritis. RhB is difficult to degrade.[12] To date, numerous treatment techniques have been researched to remove water contaminants, including physical, biological, and semiconductor-based photocatalysis.[13,14] Among these methods, semiconductor catalysis has attracted much attention as a "green", energy-saving, and economically advanced oxidation process.[15] An essential requirement for the catalyst is that semiconductor materials have a suitable band gap and show high photocatalytic performance. As one of the most important classical materials, TiO_2 has been extensively considered for the photodegradation of organic pollutants. However, due to its higher band gap (3.2 eV), it is active only in the ultraviolet (UV) or near-ultraviolet region (~4% of the sunlight spectrum).[16,17] To extend the use of sunlight, it is important to enhance photocatalysis in the visible region.

The photocatalytic activity of nanoparticles is particularly important for improving the degradation efficiency of many catalysts, including metal oxides, carbides, sulfides, chalcogenides, oxyhalides, halides, and hydroxides.[18–20] Among all semiconductor metal oxides, SnO_2,[21] ZnO_2,[22] CeO_2,[23] SiO_2,[24] MnO_2,[25] ZrO_2,[26] and TiO_2 (ref. 27 and 28) are described as developing photocatalysts due to their excellent photocatalytic activity. To

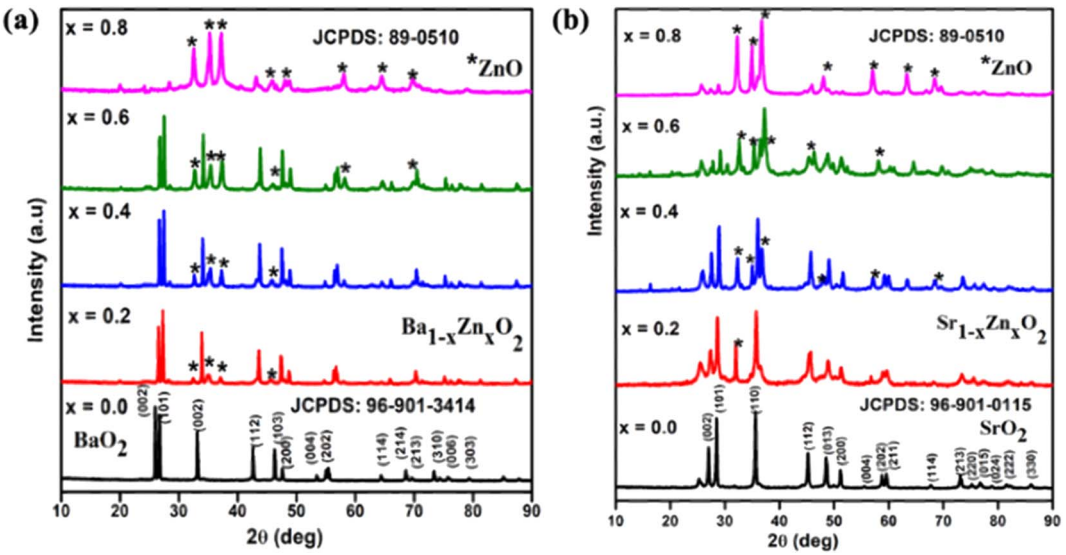

Fig. 1 XRD patterns of (a) $Ba_{1-x}Zn_xO_2$ and (b) $Sr_{1-x}Zn_xO_2$, $x = 0.2, 0.4, 0.6, 0.8$.

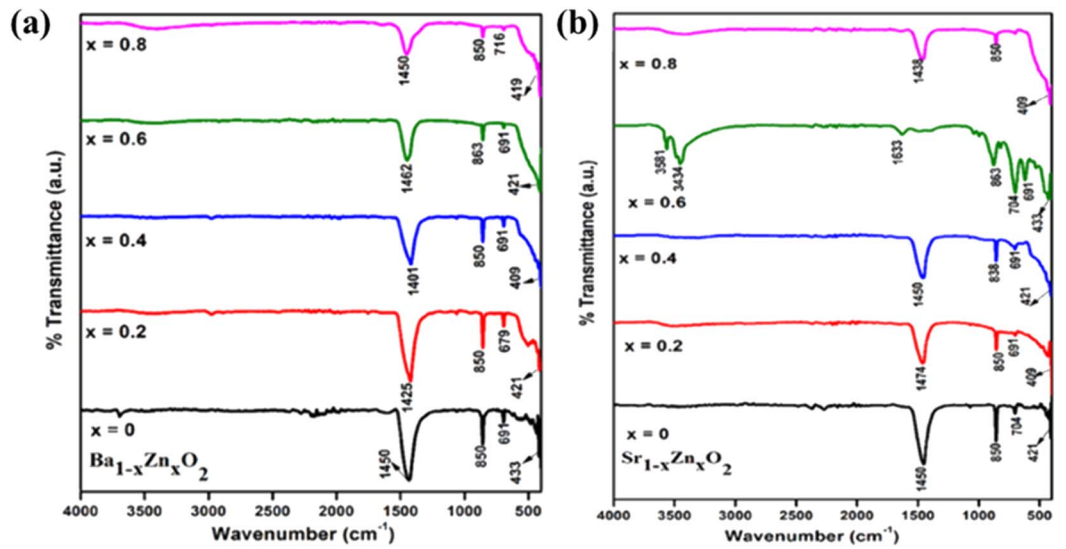

Fig. 2 FT-IR spectra of (a) $Ba_{1-x}Zn_xO_2$ and (b) $Sr_{1-x}Zn_xO_2$ $x = 0.2, 0.4, 0.6, 0.8$.

improve photocatalytic performance, many researchers focus on metal or nonmetal doping, surface modification, heterostructure formation, and composite materials. In particular, doped nanomaterials can improve structural, optical, electrical, magnetic, catalytic, and antibacterial activities.[21,26,29,30] There is always a need to develop photocatalysts that work under natural sunlight so that the process is economical. Towards this objective, we attempt to study the photocatalytic activity of barium peroxide and strontium peroxide through zinc doping.

In the present work, zinc-doped barium peroxide ($Ba_{1-x}Zn_xO_2$ $x = 0$, 0.2, 0.4, 0.6, and 0.8) and zinc-doped strontium peroxide ($Sr_{1-x}Zn_xO_2$ $x = 0$, 0.2, 0.4, 0.6, and 0.8) were developed as photocatalysts to improve the catalytic performance of barium peroxide and strontium peroxide. These photocatalysts

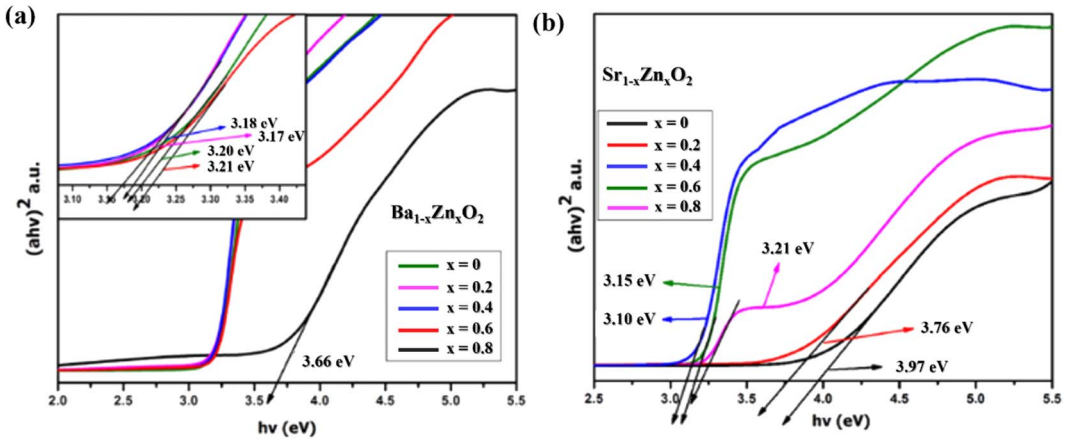

Fig. 3 of (a) $Ba_{1-x}Zn_xO_2$ and (b) $Sr_{1-x}Zn_xO_2$.

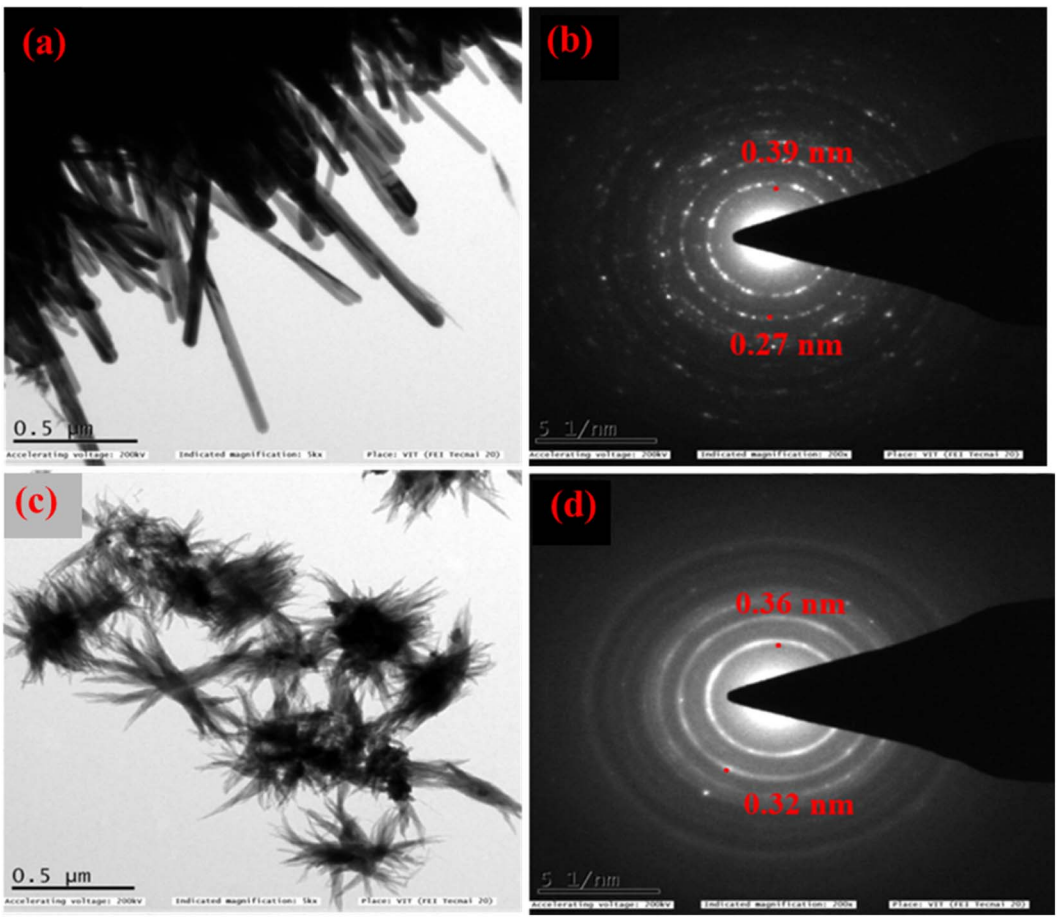

Fig. 4 HRTEM and SAED images of (a and b) $Ba_{0.4}Zn_{0.6}O_2$ and (c and d) $Sr_{0.6}Zn_{0.4}O_2$.

were prepared by the co-precipitation method. The prepared compounds were analyzed by powder X-ray diffraction (XRD), UV-vis-differential reflectance spectroscopy (UV-DRS), Fourier transform infrared spectroscopy (FT-IR), high resolution-transmission electron microscopy (HR-TEM), X-ray photoelectron spectroscopy (XPS), and Brunauer–Emmett–Teller analysis (BET). The photocatalytic performance was determined by the degradation of the dye RhB under UV and sunlight. Zinc-doped barium peroxide ($x = 0.6$) and strontium peroxide ($x = 0.4$) photocatalysts show 99.9 and 99.8% degradation in about 15 and 10 minutes, respectively, under UV light. These compositions exhibit 99.5 and 99.8% degradation efficiency within 90 minutes under sunlight irradiation. Among the studied compositions, $Ba_{0.4}Zn_{0.6}O_2$ and $Sr_{0.6}Zn_{0.4}O_2$ photocatalysts are found to be more active and efficient than well-known catalysts for RhB degradation. Zn doping into Ba & Sr peroxides has enhanced the photocatalytic activity significantly.

Experimental section

Synthesis of Zn-doped BaO_2 and Zn-doped SrO_2

All chemical reagents (99.9% pure) were purchased from S D Fine Ltd, Chennai, India, and used without further purification. The zinc-doped barium peroxides ($Ba_{1-x}Zn_xO_2$, $x = 0$, 0.2, 0.4, 0.6, and 0.8) and the zinc-doped strontium peroxides ($Sr_{1-x}Zn_xO_2$, $x = 0$, 0.2, 0.4, 0.6, and 0.8) were prepared by co-precipitation. Stoichiometric ratios of barium chloride ($BaCl_2$) or strontium chloride ($SrCl_2$) and zinc chloride ($ZnCl_2$) were added to 1 M Na_2O_2 under ice-cold conditions under an N_2 atmosphere. Then the solution was stirred for 0.5 h. The precipitate from the slurry was filtered and washed well with deionized water and dried for 12 h at 100 °C.

Characterization

The phase purity of the photocatalyst was checked by powder X-ray diffraction (XRD, D8 advance, BRUKER Germany, source: 2.2 kW Cu anode ceramic tube) in the 2θ range of 10°–90°. In transmission mode, Fourier transform infrared spectra were recorded with a SHIMADZU in the range of 400–4000 cm^{-1}. Diffuse reflectance spectroscopy of the photocatalysts was performed using a JASCO-V670 spectrophotometer in the range of 200–2500 nm. The particle size and morphology of the synthesized samples were studied using a high-resolution transmission electron microscope (HR-TEM, 200 kV FEI -Tecnai G2 20 S- TWIN) and X-ray photoelectron spectroscopy (XPS, PHI 5000 versa prob II, FEI Inc). The concentration of rhodamine B

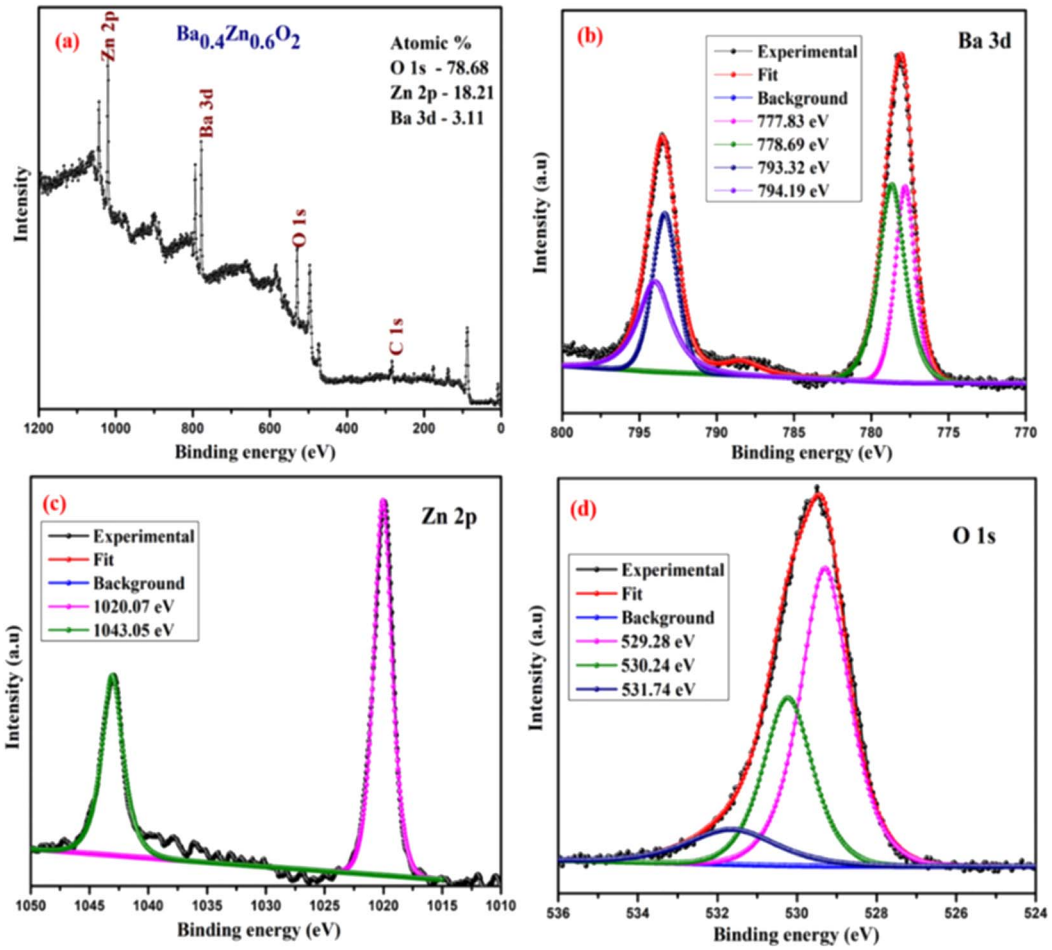

Fig. 5 XPS spectra, (a) survey scan of (b) Ba 3d, (c) Zn 2p and (d) O 1s of $Ba_{0.4}Zn_{0.6}O_2$.

for the dye degradation study was analyzed by UV-vis spectroscopy employing a JASCO V-730 model UV-visible spectrophotometer. Inductively coupled plasma – optical emission spectroscopy spectra were recorded on a PerkinElmer Avio 220 to get the bulk chemical composition.

Photocatalytic performance

The photocatalytic performance of zinc-doped barium peroxide ($Ba_{1-x}Zn_xO_2$, x = 0, 0.2, 0.4, 0.6, and 0.8) and zinc-doped strontium peroxide ($Sr_{1-x}Zn_xO_2$, x = 0, 0.2, 0.4, 0.6, and 0.8) was evaluated through the photodegradation study of RhB under irradiation with UV light (250 W Xe lamp, 365 nm wavelength) and natural sunlight. The synthesized photocatalyst (25 mg) was suspended in 50 ml of RhB (10 ppm) dye solution. The suspension was magnetically stirred for 60 min in the dark to reach equilibrium. Then the suspension was irradiated with UV light. Similarly, the suspension was exposed to natural sunlight. During the experiment, 3 ml of the aqueous solution was taken periodically and centrifuged to remove the photocatalyst particles. The absorbance of the filtrates of the dye solutions at 554 nm was recorded using a JASCO V-730 model UV-visible spectrophotometer. Dye solution without the catalyst was used as a control to negate the effect of light on the dye. The degradation rate is calculated using the formula, Degradation rate (%) = $(C_0 - C_t)/C_0 \times 100$ where C_0 is the initial concentration of the dye and C_t is the concentration of the dye at time t.

H_2O_2 estimation

H_2O_2 generated was estimated by $KMnO_4$ redox titrations. A known quantity of the catalyst was suspended in 50 ml of water. Then, calculated amounts of $KMnO_4$ and H_2SO_4 were added. It was kept under constant stirring. At regular intervals, 5 ml aliquots were withdrawn and filtered through a membrane filter. H_2O_2 was estimated by a standard back titration.

Results and discussion

Characterization of materials

The powder XRD patterns of zinc-doped barium peroxide ($Ba_{1-x}Zn_xO_2$, x = 0, 0.2, 0.4, 0.6, and 0.8) and zinc-doped strontium peroxide ($Sr_{1-x}Zn_xO_2$, x = 0, 0.2, 0.4, 0.6, and 0.8) are shown in Fig. 1a and b, respectively. The synthesized compounds crystallize in a tetragonal structure with space group $I4/mmm$ (BaO_2 (ICDD No.: 96-901-3414) and SrO_2 (ICDD No.: 96-901-0115)). In addition, the phase formation of MO_2 (M

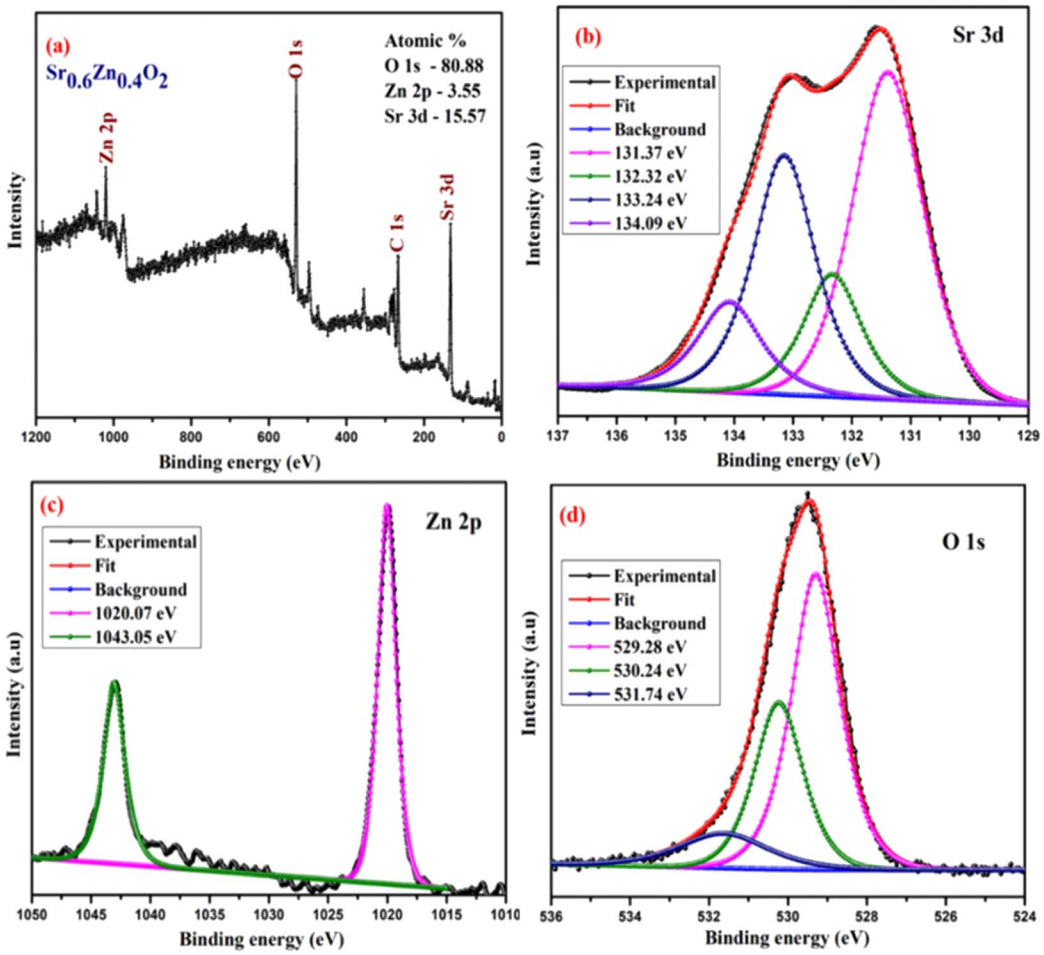

Fig. 6 XPS spectra, (a) survey scan of (b) Sr 3d, (c) Zn 2p and (d) O 1s of $Sr_{0.6}Zn_{0.4}O_2$.

= Ba and Sr) was confirmed by Rietveld refinement using the atomic parameters of BaO_2 and SrO_2 as the starting materials.[31] Fig. S1a and b† show the refined patterns of BaO_2 and SrO_2, respectively. The structural parameters of MO_2 (M = Ba and Sr) are given in Table S1.† The lattice parameters are $a = 3.81(3)$ Å, $c = 6.85(2)$ Å for BaO_2 and $a = 3.57(3)$ Å, $c = 6.63(4)$ Å for SrO_2.

The difference in lattice parameters results from the smaller ionic radius of Sr^{2+} ($r_{Sr} = 1.18$ Å) than Ba^{2+} ($r_{Ba} = 1.35$ Å).[32] It is to be noted that we could obtain phase pure BaO_2 and SrO_2 without the carbonate impurity by carrying out the reaction in a nitrogen atmosphere. From Fig. 1a and b, for $x = 0.2$ and above, it can be seen that the ZnO phase is present in addition to BaO_2 and SrO_2. The peaks marked with a star symbol indicate the presence of ZnO and the products are a composite of peroxide and ZnO in the composition range of $x = 0.2$ to 0.8 The crystallite size of the synthesized compounds was calculated using Scherrer's equation.[33] The sizes of pure BaO_2 and SrO_2 are 45 nm and 36 nm, respectively. The crystal structure of MO_2 (M = Ba and Sr) is shown in Fig. S2† using the software VESTA. The crystal structures of both compounds are isostructural to those reported by Bernal *et al.*[31] for BaO_2 and SrO_2.

The FT-IR spectra of zinc-doped barium peroxide ($Ba_{1-x}Zn_xO_2$, $x = 0$, 0.2, 0.4, 0.6, and 0.8) and zinc-doped strontium peroxide ($Sr_{1-x}Zn_xO_2$, $x = 0$, 0.2, 0.4, 0.6, and 0.8) are shown in Fig. 2a and b, respectively. The M–O stretching is observed in the frequency range of 400–900 cm^{-1}. The bands at 1400–1475 cm^{-1} confirm the O_2^{2-} species,[34] 830–864 cm^{-1} (O–Ba–O and O–Sr–O stretching modes),[35–37] 690–720 cm^{-1}, and 400–430 cm^{-1} (Ba–O, Sr–O and Zn–O bending modes).[34–37] ICP-OES confirms the bulk compositions (Table S2†).

The optical absorption spectra of zinc-doped barium peroxide ($Ba_{1-x}Zn_xO_2$, $x = 0$, 0.2, 0.4, 0.6, and 0.8) and zinc-doped strontium peroxide ($Sr_{1-x}Zn_xO_2$, $x = 0$, 0.2, 0.4, 0.6, and 0.8) were studied by UV-DRS analysis. The band gap (eV) of the synthesized products was calculated using Tauc's equation.[34] Fig. 3a and b show that the band gaps of $Ba_{1-x}Zn_xO_2$, $x = 0$, 0.2, 0.4, 0.6, 0.8 and $Sr_{1-x}Zn_xO_2$, $x = 0$, 0.2, 0.4, 0.6, 0.8 are in the range of 3.66 to 3.20 eV and 3.97 to 3.21 eV, respectively.

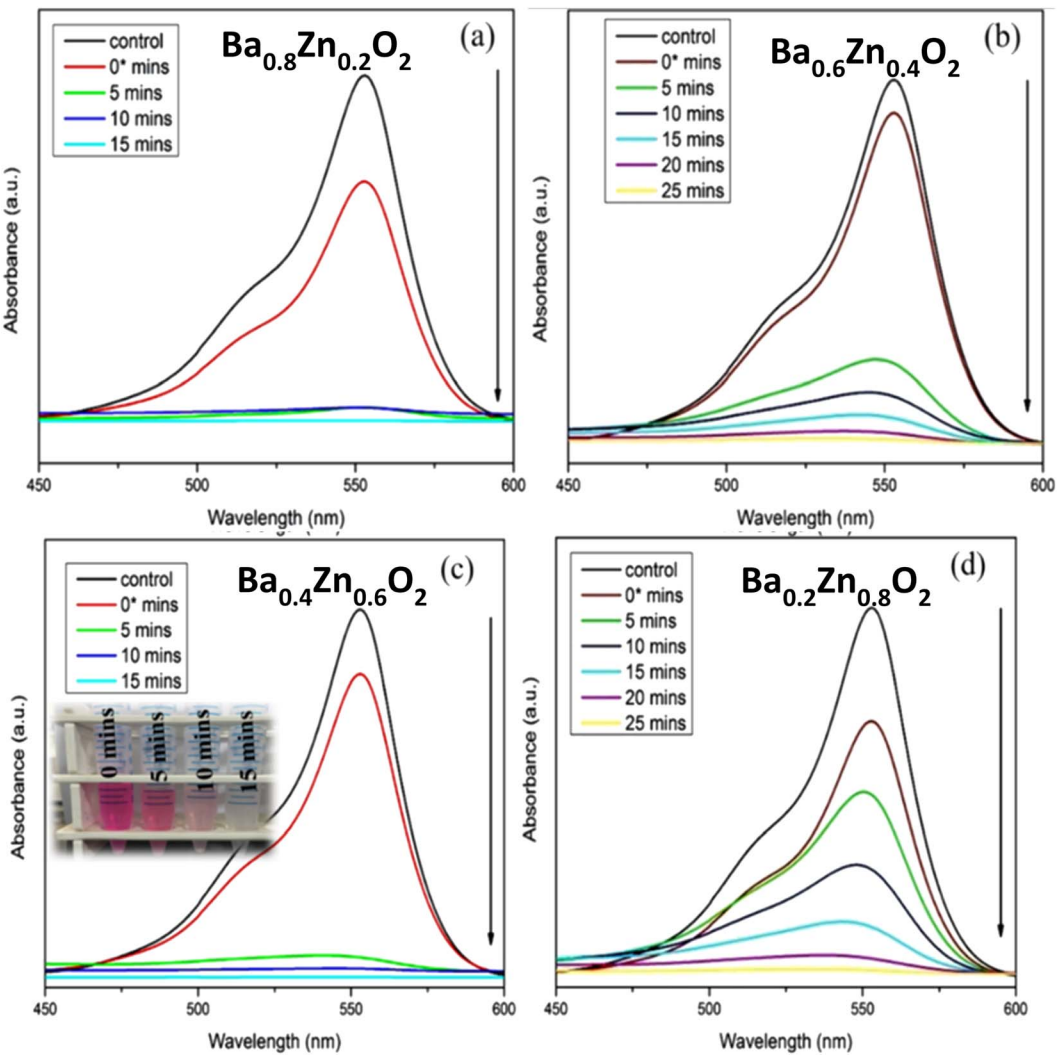

Fig. 7 Influence of Zn doping on the photocatalytic degradation of RhB using (a) $Ba_{0.8}Zn_{0.2}O_2$, (b) $Ba_{0.6}Zn_{0.4}O_2$, (c) $Ba_{0.4}Zn_{0.6}O_2$ and (d) $Ba_{0.2}Zn_{0.8}O_2$ photocatalysts under UV light irradiation.

For further characterization (HR-TEM, XPS, and BET) we chose the low band gap materials $Ba_{0.4}Zn_{0.6}O_2$ and $Sr_{0.6}Zn_{0.4}O_2$. The HR-TEM analysis was carried out to investigate the size and shape of $Ba_{0.4}Zn_{0.6}O_2$ and $Sr_{0.6}Zn_{0.4}O_2$ particles (Fig. 4a–d). The morphology of $Ba_{0.4}Zn_{0.6}O_2$ shows the shape of rods (Fig. 4a) and $Sr_{0.6}Zn_{0.4}O_2$ has a flower-like morphology (Fig. 4c) respectively. The selected area electron diffraction (SAED) (Fig. 4b and d) image shows that the *d*-spacing is 0.39 nm and 0.27 nm and 0.36 nm and 0.32 nm, corresponding to $Ba_{0.4}Zn_{0.6}O_2$ and $Sr_{0.6}Zn_{0.4}O_2$ phases.

The surface chemical composition and bonding states of the $Ba_{0.4}Zn_{0.6}O_2$ and $Sr_{0.6}Zn_{0.4}O_2$ photocatalysts were analyzed by XPS. Fig. 5 and 6 show the XPS spectra of $Ba_{0.4}Zn_{0.6}O_2$ and $Sr_{0.6}Zn_{0.4}O_2$ samples showing peaks of Zn 2p, Ba 3d, Sr 3d, O 1s, and C 1s. The C 1s binding energy was used to calibrate all binding energies (C 1s: 283.4 eV). The deconvolution method is used for the Zn, Ba, Sr, and O elements. Ba 3d (Fig. 5b) contains two spin–orbit doublets Ba $3d_{5/2}$ (777.83 eV and 778.69 eV) and Ba $3d_{3/2}$ (793.32 eV and 794.19), confirming the presence of Ba^{2+} ions.[38,39] The XPS spectrum of Sr 3d is shown in Fig. 6b, with four peaks at 131.37 eV and 132.32 eV and 133.24 eV and 134.09 eV related to Sr $3d_{5/2}$ and Sr $3d_{3/2}$ of Sr^{2+}.[37,40] Zn 2*p* is shown in Fig. 5c and 6c, and Zn $2p_{3/2}$ (1020.07 eV) and Zn $2p_{1/2}$ (1043.05 eV) confirm the presence of Zn^{2+} ions in both compounds.[34,41] The binding energy of the O 1s peak (Fig. 5d and 6d) was found to be 529.28 eV, 530.24 eV, and 531.74 eV, which are related to the lattice oxygen in the metal–oxygen bonds, hydroxyl species, and O_2^{2-} species, respectively.[34,37,41,42]

Table 1 Photocatalytic performance of the catalysts

	$Ba_{1-x}Zn_xO_2$		$Sr_{1-x}Zn_xO_2$	
Composition (*x*)	Time (min)	% of degradation	Time (min)	% of degradation
0	35	98.5	35	98.5
0.2	20	98.6	30	98.6
0.4	25	99	10	99.8
0.6	15	99.9	15	99.2
0.8	25	97.6	20	98.5

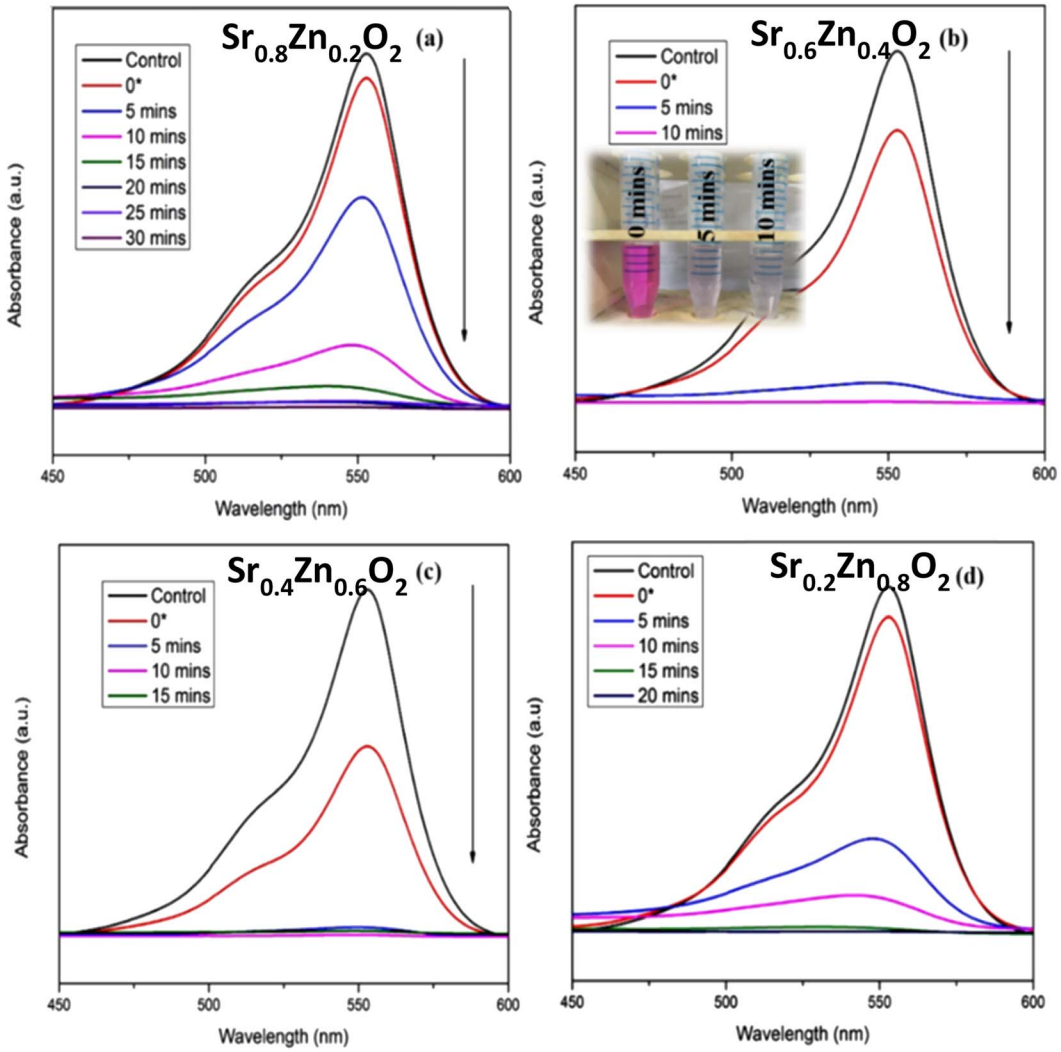

Fig. 8 Influence of Zn doping on the photocatalytic degradation of RhB using (a) $Sr_{0.8}Zn_{0.2}O_2$, (b) $Sr_{0.6}Zn_{0.4}O_2$, (c) $Sr_{0.4}Zn_{0.6}O_2$, and (d) $Sr_{0.2}Zn_{0.8}O_2$ photocatalysts under UV light irradiation.

One of the main factors on which the photocatalytic performance depends is the surface area of the catalyst. BET surface areas of BaO_2, SrO_2, $Ba_{0.4}Zn_{0.6}O_2$, and $Sr_{0.6}Zn_{0.4}O_2$ samples are 2.2, 3.4, 13.5, and 18.3 $m^2\ g^{-1}$, respectively. Zinc-doped barium peroxide and strontium peroxide have a larger surface area with smaller particles.

The present study deals with the degradation of RhB, an organic pollutant, using BaO_2, $Ba_{0.8}Zn_{0.2}O_2$, $Ba_{0.6}Zn_{0.4}O_2$, $Ba_{0.4}Zn_{0.6}O_2$, and $Ba_{0.2}Zn_{0.8}O_2$ and SrO_2, $Sr_{0.8}Zn_{0.2}O_2$, $Sr_{0.6}Zn_{0.4}O_2$, $Sr_{0.4}Zn_{0.6}O_2$, and $Sr_{0.2}Zn_{0.8}O_2$ photocatalysts under UV and direct sunlight. For the model reaction, 25 mg of the different photocatalysts and 50 ml of a 10 ppm RhB dye solution were examined with a photocatalytic instrument under UV light irradiation. Fig. S3†, 7a–d & Table 1 show the efficiency of RhB dye degradation using the $Ba_{1-x}Zn_xO_2$ photocatalysts.

From Table 1, it is evident that all the compositions degrade the dye more than 95% within a short duration; in particular the compositions $Ba_{0.4}Zn_{0.6}O_2$ and $Sr_{0.6}Zn_{0.4}O_2$ exhibit faster degradation. This may be due to the high surface area. The amount of H_2O_2 released from the aqueous suspension is tabulated in Table S3.† It is to be noted that the best compositions $Ba_{0.4}Zn_{0.6}O_2$ and $Sr_{0.6}Zn_{0.4}O_2$ release the highest amount

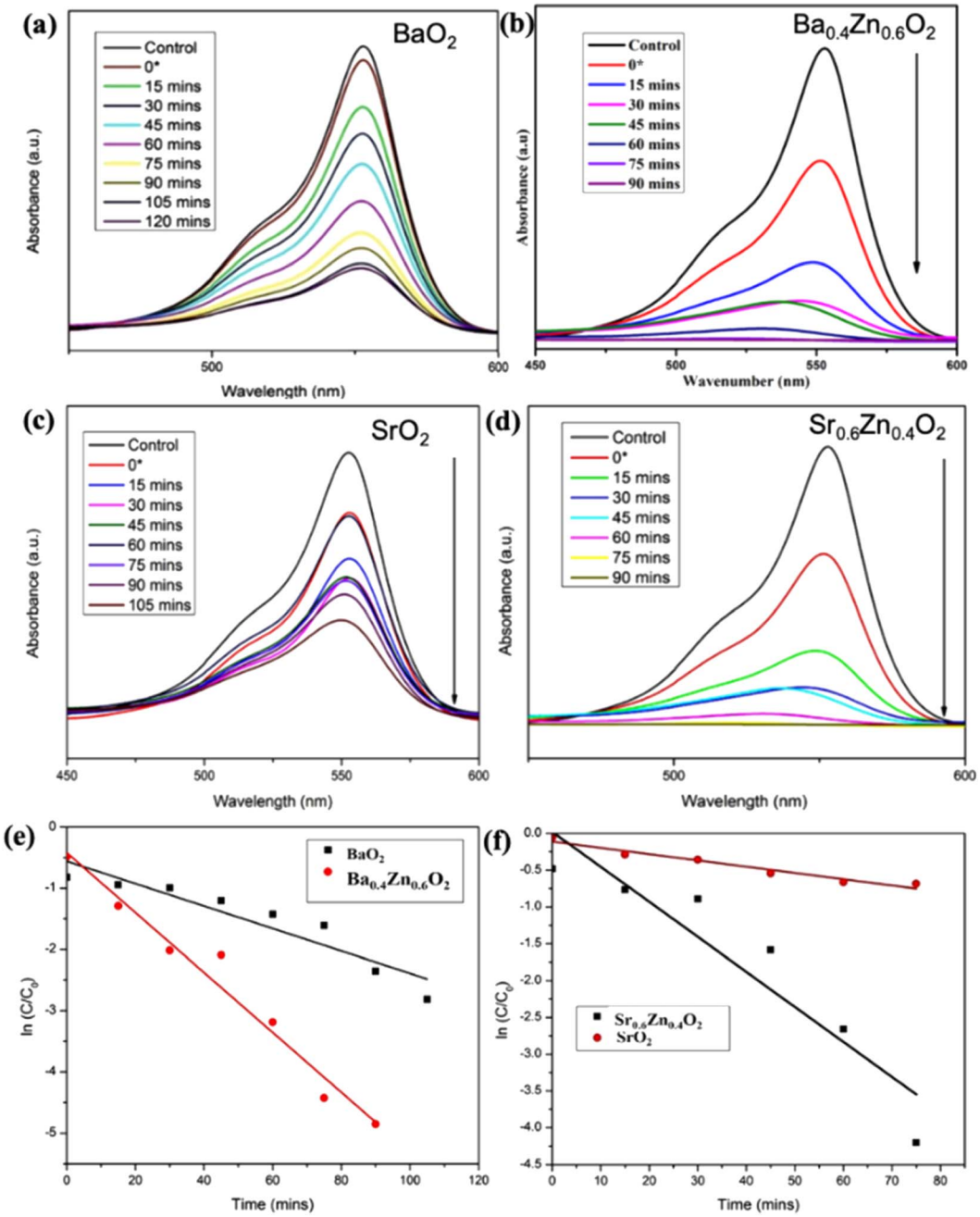

Fig. 9 The photocatalytic degradation efficiency of RhB by (a) BaO_2, (b) $Ba_{0.4}Zn_{0.6}O_2$ (c) SrO_2 and (d) $Sr_{0.6}Zn_{0.4}O_2$ photocatalysts under direct sunlight. First-order-kinetics plots of RhB degradation using (e) BaO_2 and $Ba_{0.4}Zn_{0.6}O_2$ and (f) SrO_2.

of H_2O_2 confirming that the photocatalytic activity is maximum in these compositions.

The photocatalytic performance of $Sr_{1-x}Zn_xO_2$ against the RhB dye under UV light is shown in Fig. S4†, 8a–d & Table 1. The composition $x = 0.4$ shows the fastest degradation. From the results, we conclude that zinc doping enhances the performance of the photocatalyst. Fig. S5† shows the first-order pseudo-kinetics for the photocatalytic degradation of RhB by BaO_2, $Ba_{0.4}Zn_{0.6}O_2$, and SrO_2, $Sr_{0.6}Zn_{0.4}O_2$ photocatalysts under UV light illumination. The rate constants, k, calculated for BaO_2, $Ba_{0.4}Zn_{0.6}O_2$ photocatalysts are 0.082 and 0.344 min^{-1}, respectively (Fig. S5a†). As shown in Fig. S5b,† the rate constants for SrO_2 and $Sr_{0.6}Zn_{0.4}O_2$ are 0.099 and 0.394 min^{-1} respectively. Compared with the undoped peroxides, the $Ba_{0.4}Zn_{0.6}O_2$ and $Sr_{0.6}Zn_{0.4}O_2$ photocatalysts exhibit four times faster kinetics.

The photocatalysts $Ba_{0.4}Zn_{0.6}O_2$ and $Sr_{0.6}Zn_{0.4}O_2$ exhibit higher photocatalytic performance for the degradation of RhB (Table S4†) under UV light compared with other systems reported in the literature. The rate constants are two orders of magnitude higher in the peroxide composite system. This is associated with the interface of peroxide and ZnO. Therefore, BaO_2, $Ba_{0.4}Zn_{0.6}O_2$, SrO_2, and $Sr_{0.6}Zn_{0.4}O_2$ photocatalysts were selected for photocatalytic degradation of RhB under direct sunlight. According to Fig. 9a–d, the photocatalytic degradation of RhB with the photocatalysts BaO_2 and $Ba_{0.4}Zn_{0.6}O_2$, and SrO_2 and $Sr_{0.6}Zn_{0.4}O_2$ is 50.2% after 120 minutes and 99.8% after 90 minutes and 60.5% after 105 minutes and 99.5% after 90 minutes respectively under direct sunlight. This may be due to large surface area and a higher amount of H_2O_2. In addition, the photodegradation kinetics of RhB by BaO_2, $Ba_{0.4}Zn_{0.6}O_2$, and SrO_2, $Sr_{0.6}Zn_{0.4}O_2$ photocatalysts under sunlight are shown in Fig. 9e and f, respectively. The rate constants (k) for $Ba_{0.4}Zn_{0.6}O_2$ and $Sr_{0.6}Zn_{0.4}O_2$, are 2.480 and 2.340 min^{-1} respectively which are two orders of magnitude higher compared to those for BaO_2 and SrO_2 (0.018 and 0.020 min^{-1}, respectively). The higher activity of the doped samples may also be due to the more efficient generation of electron–hole pairs under sunlight.[43] From the results, we conclude that the compositions $Ba_{0.4}Zn_{0.6}O_2$ and $Sr_{0.6}Zn_{0.4}O_2$ are suitable photocatalysts for degradation by sunlight. These photocatalysts exhibit high photocatalytic performance in direct sunlight compared to previous reports (Table S5†). This finding can be used for a wide range of environmental remediation applications.

To understand the photocatalytic performance of $Ba_{0.4}Zn_{0.6}O_2$ and Sr0.6Zn0.4O2 photocatalysts, a possible mechanism is proposed as shown in Scheme 1. The general mechanism involves excitation of electrons from the valence band (VB) to the conduction band (CB) resulting in holes in the VB and electrons in the CB.[44] Holes and electrons react with water and oxygen producing $^{\bullet}OH$ radicals and super oxide radicals respectively that could degrade the dyes. The various steps are given in eqn (1)–(7).

$$MO_2 + h\nu \rightarrow e^- (CB) + h^+ (VB) \quad (1)$$

$$H_2O + h^+ \rightarrow {}^{\bullet}OH + H^+ \quad (2)$$

$$O_2 + e^- \rightarrow O_2^{-\bullet} \quad (3)$$

$$O_2^{-\bullet} + H^+ \rightarrow HO_2^{\bullet} \quad (4)$$

$$2HO_2^{\bullet} \rightarrow H_2O_2 + O_2^{-\bullet} \quad (5)$$

$$2{}^{\bullet}OH \rightarrow H_2O_2 \quad (6)$$

$$H_2O_2 + e^- \rightarrow OH^- + {}^{\bullet}OH \quad (7)$$

Doping of Zn into the peroxides creates additional levels below the conduction bands of BaO_2 and SrO_2 similar to doped ZnO.[45]

Metal peroxides in aqueous suspensions release hydrogen peroxide. The released hydrogen peroxide could be decomposed under UV light and sunlight into hydroxyl radicals that degrade the dye. Thus, the composites of peroxide could degrade dyes through the chemical route and photochemical routes. Moreover, hydrogen peroxide is a scavenger of the e^- from zinc that is present on the surface of BaO_2 and SrO_2, forming hydroxyl radicals and hydroxyl ions. The highly reactive hydroxyl radical and O_2^- are responsible for the photochemical degradation of RhB, which is degraded to non-toxic products such as carbon dioxide and water.

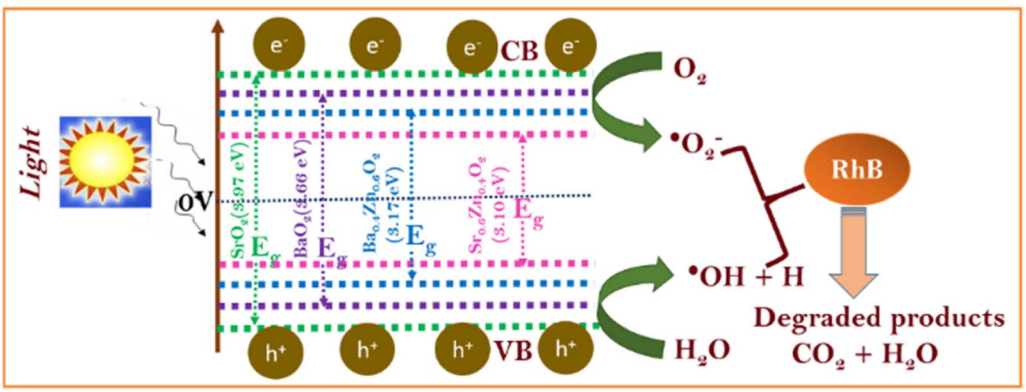

Scheme 1 Photocatalytic mechanism of BaO_2, $Ba_{0.4}Zn_{0.6}O_2$, SrO_2, and $Sr_{0.6}Zn_{0.4}O_2$.

Degradation pathway

From the literature it is proven that RhB degradation predominantly occurred *via* chromophore cleavage resulting in 18 small molecules (mainly organic acids and alcohols), confirmed by GC – MS, that mineralize into CO_2 and H_2O.[46]

Reusability

To ascertain the stability and reusability of the catalysts for dye degradation, catalysts after dye degradation were centrifuged, washed with water and dried in an oven at 60 °C. The dried powder was re-used for degradation. This cycle is repeated 3 times. Fig. S6† shows that the catalysts are stable and reusable.

Conclusions

In summary, we have successfully prepared and characterized BaO_2 and SrO_2 and their composites with ZnO and tested their photocatalytic activity against the organic pollutant RhB dye under UV and sunlight irradiation. The compositions $Ba_{0.4}Zn_{0.6}O_2$ and $Sr_{0.6}Zn_{0.4}O_2$ as photocatalysts show higher photocatalytic performance. Zn doped peroxides exhibit higher photocatalytic activity than the pure peroxides both under UV-light and sunlight. The rate constants, k, of $Ba_{0.4}Zn_{0.6}O_2$ and $Sr_{0.6}Zn_{0.4}O_2$ for degradation are two orders of magnitude higher than those of the undoped photocatalysts under sunlight. Moreover, the doped catalysts perform better than known catalysts under UV and sunlight irradiation.

Author contributions

K. V. S. performed part of the experiments, analyzed the data, and wrote the manuscript. D. B. performed part of the experiments and analyzed the data. N. S. performed part of the experiments and analyzed the data. M. B. analyzed the experimental data. M. R. analyzed the characterization and photocatalytic experimental data. G. K. D. and A. R. P. S. analyzed the experimental data. S. S. designed the photocatalytic experiment. K. V. K. designed the photocatalytic experiment. V. R. got the idea for this topic.

Conflicts of interest

There are no conflicts to declare.

Acknowledgements

The work was supported by the Grant DST-SERB (No. EMR/2016/007152). The authors thank VIT for providing 'VIT SEED GRANT (RGEMS) – Sanction Order no: SG20230024' for carrying out this research work.

Notes and references

1 H. T. Vo, A. T. Nguyen, C. Van Tran, S. X. Nguyen, N. T. Tung, D. T. Pham, D. D. Nguyen and D. D. La, *ACS Omega*, 2021, **6**, 23203–23210.
2 M. Dehghani, H. Nadeem, V. S. Raghuwanshi, H. Mahdavi, M. M. Banaszak Holl and W. Batchelor, *ACS Appl. Nano Mater.*, 2020, **3**, 10284–10295.
3 M. S. Samuel, S. Jose, E. Selvarajan, T. Mathimani and A. Pugazhendhi, *J. Photochem. Photobiol., B*, 2020, **202**, 111642.
4 M. S. Samuel, J. Bhattacharya, C. Parthiban, G. Viswanathan and N. D. Pradeep Singh, *Ultrason. Sonochem.*, 2018, **49**, 215–221.
5 M. S. Samuel, S. Suman, Venkateshkannan, E. Selvarajan, T. Mathimani and A. Pugazhendhi, *J. Photochem. Photobiol., B*, 2020, **204**, 111809.
6 I. Karuppusamy, M. S. Samuel, E. Selvarajan, S. Shanmugam, P. Sahaya Murphin Kumar, K. Brindhadevi and A. Pugazhendhi, *J. Colloid Interface Sci.*, 2021, **584**, 770–778.
7 M. S. Samuel, E. Selvarajan, T. Mathimani, N. Santhanam, T. N. Phuong, K. Brindhadevi and A. Pugazhendhi, *J. Photochem. Photobiol., B*, 2020, **211**, 112011.
8 M. S. Samuel, K. V. Savunthari and S. Ethiraj, *Environ. Sci. Pollut. Res.*, 2021, **28**, 40835–40843.
9 K. Iqbal, A. Iqbal, A. M. Kirillov, W. Liu and Y. Tang, *Inorg. Chem.*, 2018, **57**, 13270–13278.
10 K. Iqbal, A. Iqbal, A. M. Kirillov, C. Shan, W. Liu and Y. Tang, *J. Mater. Chem. A*, 2018, **6**, 4515–4524.
11 X. Luo, R. Abazari, M. Tahir, W. K. Fan, A. Kumar, T. Kalhorizadeh, A. M. Kirillov, A. R. Amani-Ghadim, J. Chen and Y. Zhou, *Coord. Chem. Rev.*, 2022, **461**, 214505.
12 X. H. Li, Y. Liu, H. Y. Lin, N. Xu, Z. Zhang, G. C. Liu and X. L. Wang, *Cryst. Growth Des.*, 2022, **22**, 3845–3852.
13 Y. Li, B. Wu, G. Zhu, Y. Liu, W. J. Ng, A. Appan and S. K. Tan, *Sci. Total Environ.*, 2016, **562**, 604–613.
14 Y. Bao, W. J. Lee, J. Z. Y. Seow, H. Hara, Y. N. Liang, H. Feng, J. Z. Xu, T. T. Lim and X. Hu, *ACS ES&T Water*, 2021, **1**, 837–846.
15 A. Kubacka, M. Fernández-García and G. Colón, *Chem. Rev.*, 2012, **112**, 1555–1614.
16 M. Dahl, Y. Liu and Y. Yin, *Chem. Rev.*, 2014, **114**, 9853–9889.
17 L. T. Nyamutswa, B. Hanson, D. Navaratna, S. F. Collins, K. G. Linden and M. C. Duke, *ACS ES&T Water*, 2021, **1**, 2001–2011.
18 A. Malathi, P. Arunachalam, A. N. Grace, J. Madhavan and A. M. Al-Mayouf, *Appl. Surf. Sci.*, 2017, **412**, 85–95.
19 A. Malathi, V. Vasanthakumar, P. Arunachalam, J. Madhavan and M. A. Ghanem, *J. Colloid Interface Sci.*, 2017, **506**, 553–563.
20 Z. Qiao, T. Yan, W. Li and B. Huang, *New J. Chem.*, 2017, **41**, 3134–3142.
21 A. Ahmed, M. Naseem Siddique, U. Alam, T. Ali and P. Tripathi, *Appl. Surf. Sci.*, 2019, **463**, 976–985.
22 C. C. Hsu and N. L. Wu, *J. Photochem. Photobiol. A*, 2005, **172**, 269–274.
23 R. Bakkiyaraj, M. Balakrishnan, G. Bharath and N. Ponpandian, *J. Alloys Compd.*, 2017, **724**, 555–564.
24 C. Anastasescu, M. Zaharescu, D. Angelescu, C. Munteanu, V. Bratan, T. Spataru, C. Negrila, N. Spataru and I. Balint, *Sol. Energy Mater. Sol. Cells*, 2017, **159**, 325–335.

25 A. Mehta and S. Basu, *J. Photochem. Photobiol. A*, 2017, **343**, 1–6.
26 C. V. Reddy, I. N. Reddy, J. Shim, D. Kim and K. Yoo, *Ceram. Int.*, 2018, **44**, 12329–12339.
27 F. Pellegrino, L. Pellutiè, F. Sordello, C. Minero, E. Ortel, V. D. Hodoroaba and V. Maurino, *Appl. Catal., B*, 2017, **216**, 80–87.
28 A. D. McQueen, M. L. Ballentine, L. R. May, C. H. Laber, A. Das, M. J. Bortner and A. J. Kennedy, *ACS ES&T Water*, 2022, **2**, 137–147.
29 A. Zafar, A. ur Rahman, S. Shahzada, S. Anwar, M. Khan, A. Nisar, M. Ahmad and S. Karim, *J. Alloys Compd.*, 2017, **727**, 683–690.
30 V. Shanmugam and K. S. Jeyaperumal, *Appl. Surf. Sci.*, 2018, **449**, 617–630.
31 J. D. Bernal, E. Djatlowa, I. Kasarnowsky, S. Reichstein and A. G. Ward, *Z. fur Krist. - Cryst. Mater.*, 1935, **92**, 344–354.
32 R. D. Shannon, *Acta Crystallogr. B*, 1976, **32**, 751–767.
33 V. S. Kiran and S. Sumathi, *J. Magn. Magn. Mater.*, 2017, **421**, 113–119.
34 V. Lakshmi Prasanna and V. Rajagopalan, *Sci. Rep.*, 2016, **6**, 1–10.
35 R. Gomes, S. Roming, A. Przybilla, M. A. R. Meier and C. Feldmann, *J. Mater. Chem. C*, 2014, **2**, 1513–1518.
36 M. Kumar Trivedi, R. M. Tallapragada and A. Branton, *J. Lasers Opt. Photonics*, 2015, **2**, 1000122.
37 K. Prakash, P. S. Kumar, P. Latha, K. Stalin Durai, R. Shanmugam and S. Karuthapandian, *Mater. Res. Bull.*, 2017, **93**, 112–122.
38 T. C. Droubay, L. Kong, S. A. Chambers and W. P. Hess, *Surf. Sci.*, 2015, **632**, 201–206.
39 F. Alema and K. Pokhodnya, *J. Adv. Dielectr.*, 2015, **5**, 1–9.
40 S. Picozzi, C. Ma, Z. Yang, R. Bertacco, M. Cantoni, A. Cattoni, D. Petti, S. Brivio and F. Ciccacci, *J. Appl. Phys.*, 2008, **103**, 044903.
41 S. Anbarasu, S. Ilangovan, V. S. Nagarethinam, J. Srivind, S. Balamurugan, M. Suganya and A. R. Balu, *Nano-Struct. Nano-Objects*, 2019, **17**, 67–76.
42 Y. Su, W. Yang, W. Sun, Q. Li and J. K. Shang, *Chem. Eng. J.*, 2015, **268**, 270–279.
43 N. G. Yadav, L. S. Chaudhary, P. A. Sakhare, T. D. Dongale, P. S. Patil and A. D. Sheikh, *J. Colloid Interface Sci.*, 2018, **527**, 289–297.
44 F. Azeez, E. Al-Hetlani, M. Arafa, Y. Abdelmonem, A. A. Nazeer, M. O. Amin and M. Madkour, *Sci. Rep.*, 2018, **8**, 1–9.
45 A. Tabib, W. Bouslama, B. Sieber, A. Addad, H. Elhouichet, M. Férid and R. Boukherroub, *Appl. Surf. Sci.*, 2017, **396**, 1528–1538.
46 K. Yu, S. Yang, H. He, C. Sun, C. Gu and Y. Ju, *J. Phys. Chem. A*, 2009, **113**, 10024–10032.